Journal of Alloys and Compounds 509 (2011) 1328–1332

Contents lists available at ScienceDirect

Journal of Alloys and Compounds

journal homepage: www.elsevier.com/locate/jallcom

ZnO and TiO_2 1D nanostructures for photocatalytic applications

M.Y. Guo [a], M.K. Fung [a], F. Fang [a], X.Y. Chen [a], A.M.C. Ng [a], A.B. Djurišić [a,*], W.K. Chan [b]

[a] Department of Physics, The University of Hong Kong, Pokfulam Road, Hong Kong
[b] Department of Chemistry, The University of Hong Kong, Pokfulam Road, Hong Kong

ARTICLE INFO

Article history:
Received 10 June 2010
Received in revised form 5 October 2010
Accepted 7 October 2010
Available online 15 October 2010

Keywords:
Oxide materials
Photocatalysis

ABSTRACT

ZnO and TiO_2 1D nanostructures (nanorods and nanotubes) were prepared by low-cost, low-temperature, solution-based methods and their properties and photocatalytic performance were studied. ZnO nanorod samples with titania and alumina shells were also prepared by solution-based methods, and their properties and photocatalytic performance were compared to that of bare ZnO nanorods. We found that ZnO and TiO_2 exhibited comparable photocatalytic performance. Faster dye degradation under simulated solar illumination was observed for ZnO, while under UV illumination faster degradation was observed for TiO_2. ZnO nanorods with titania shells exhibited inferior photocatalytic performance, while for alumina shells the performance was similar to bare ZnO. Reasons for observed differences are discussed, and the effect of the shell on photocatalytic activity is attributed to the changes in native defects at the ZnO surface/shell interface.

1. Introduction

Photocatalysis has been intensively investigated in recent years [1–17]. In a photocatalytic process, electron–hole pairs are generated under illumination, followed by oxidation and/or reduction reactions at the surface of the photocatalyst [1]. In the presence of a photocatalyst, organic contaminants can be oxidized directly by a photogenerated hole or indirectly via reaction with reactive oxygen species (ROS), such as hydroxyl radical $OH^{\bullet}$, produced in the solution [1]. TiO_2 is a widely used photocatalyst material [1–7]. It exhibits photocatalytic activity under UV illumination [1]. Activity under solar illumination has also been reported [1], although efficiency is expected to be low since it can only absorb UV A and UV B solar radiation [2]. A number of materials have been investigated as an alternative to TiO_2, including ZnO [2,8,13–16]. ZnO exhibits similar [2] or better [8,13] activity compared to titania, but it is also less stable compared to titania [2] and susceptible to photocorrosion [8]. However, improved stability has been reported for microscale ZnO which was attributed to better crystallinity and lower defects [13]. Furthermore, photocatalytic activity of ZnO can be further enhanced [15,17] or extended into the visible spectral range [12] by doping with different elements. In addition to studies of individual ZnO and TiO_2 photocatalyst materials, ZnO/TiO_2 composites have also been reported [11,14]. Both reduced [11,14] and increased [11] photocatalytic activity was reported, and the activity was strongly dependent on the processing conditions of the composite material [11]. While there have been efforts in extending the absorption of TiO_2 and ZnO photocatalysts into the visible spectral range by various methods [3], there is also significant interest in the study of different nanostructured morphologies to improve photocatalytic activity [4,9]. In spite of intensive research on different morphologies of both ZnO and TiO_2, comparisons of the two materials are commonly performed on nanoparticle or powder samples [8,13].

In this work, we have studied the photocatalytic performance of TiO_2 nanotube arrays and ZnO nanorod arrays. These structures are of interest since it has been shown that 1D nanostructure arrays can exhibit improved performance compared to conventional thin films composed of nanoparticles [5]. For ZnO, core–shell structures have also been studied since it was reported that a shell can affect the rate of recombination of photogenerated carriers in solar cells [18] and photoelectrocatalytic water splitting [6]. In addition, the presence of a shell is expected to improve or even eliminate the problem of photocorrosion. Furthermore, since ideal photocatalysts should be inexpensive, in addition to being efficient, stable, and chemically and biologically inert [1], we have focused on low-cost, low-temperature, solution-based methods for both materials. TiO_2 nanotubes were prepared by anodization [5–7,19–21]. The tubes were annealed at 450 °C to obtain anatase phase of titania, since anatase is considered more photocatalytically active compared to rutile [2]. For ZnO nanorods, hydrothermal growth method [22,23] was used. Core–shell ZnO-based structures were also prepared by a solution-based method. The photocatalytic activity of different samples under UV and simulated solar illumination were compared and the results are discussed.

* Corresponding author.
E-mail address: dalek@hkusua.hku.hk (A.B. Djurišić).

0925-8388/$ – see front matter © 2010 Elsevier B.V. All rights reserved.
doi:10.1016/j.jallcom.2010.10.028

2. Experimental details

2.1. ZnO nanorod growth

ZnO nanorods were grown by a hydrothermal method [22,23]. Si substrates were cleaned using toluene, acetone, ethanol and then kept in mixed ammonia and H_2O_2 aqueous solution (ratio of ammonia:H_2O_2:water is 1:1:5) at 60 °C for 20 min and finally rinsed by de-ionized water. Seed layer was prepared from 5 mM solutions of zinc acetate (Aldrich, 99.99%) in ethanol (5 cycles of placing solution droplets, rinsing and drying, followed by annealing at 350 °C for 20 min, and then the entire procedure was repeated to ensure complete coverage of the substrate). The substrates with the seed layer were placed seed-side down into a solution containing 0.1 g polyethylenimine (Aldrich, 50 wt.%), 40 mM (0.56 g) zinc nitrate hydrate (Aldrich, 99.999%) and 25 mM (0.26 g) hexamethylene tetramine (HMT, Aldrich, 99 + %) in 75 ml de-ionized water. The temperature was set to 90 °C and the reaction time was 2.5 h.

2.2. Shell preparation

For alumina shell, 56.2 mg aluminum nitrate hydrate (Aldrich, 99.997%) and 0.5 g HMT were dissolved in 10 ml de-ionised water. The solution was spin-coated on ZnO nanorods at 5000 rpm for 2 min, followed by annealing in air at 200 °C for 20 min. Then the spin-coating and annealing was repeated one more time. For titania shell, the solution of 0.05 ml of titanium isopropoxide in 3 ml of ethanol was spin-coated at 5000 rpm for 2 min, followed by annealing in the air at 400 °C for 1 h.

2.3. TiO_2 nanotube preparation

Titanium foils (0.25 mm thickness) were cleaned by sonication in toluene, acetone, ethanol, and de-ionized water and then dried with N_2 gas. Then, the foils were immersed in the electrolyte consisting of 1.36 g ammonium fluoride (99 + %, BDH) and 8 ml de-ionized water in 400 ml ethylene glycol (99.8%, Aldrich) and anodization was performed for 2 h at 60 V, similar to previously reported procedures [20,21]. Annealing was performed in a tube furnace in air at 450 °C to obtain anatase titania. Anatase crystal structure for this annealing temperature was confirmed by X-ray diffraction using a X-ray diffraction (XRD) using Bruker AXS SMART CCD diffractometer. The cooling and heating rates were 1 °C/min.

2.4. Sample characterization

The morphology and structure of the samples was examined by electron microscopy using a JEOL JSM-7001F field emission scanning electron microscope (SEM) and Phillips Tecnai G2 20 S-Twin transmission electron microscope (TEM). The composition of the samples was characterized by EDX. PL measurements were performed at room temperature using a HeCd laser (325 nm) as an excitation source and the spectra were collected using a PDA-512_USB (Control Development Inc) fiberoptic spectrometer. The excitation power was 1.6 mW, corresponding to an excitation power density of ~267 mW/cm^2. Brunauer–Emmett–Teller (BET) surface area measurements were performed using a Nova 1200 Gas Sorption Analyzer (Quantachrome Corporation).

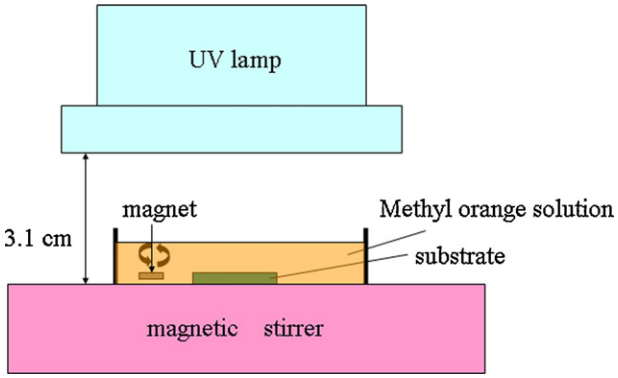

Fig. 1. Schematic diagram of the experimental setup.

2.5. Photocatalysis experiments

Schematic diagram of the experimental setup is shown in Fig. 1. Methyl orange dye (1 mg) was dissolved in 1 l of deionized (DI) water. The samples were placed into a Petri dish containing 12.5 ml of methyl orange solution and 37.5 ml of DI water and left for 15 min in the dark to achieve equilibrium. The pH of the solution was 6.7. The solution was stirred using a magnetic stirrer during UV illumination (Blak-Ray® B-100 AP Lamp, 365 nm, 66.2 mW/cm^2) and simulated solar illumination (Oriel solar simulator 81260-1000 with AM 1.0 filter) with (16.7 mW/cm^2) and without (39.5 mW/cm^2) polycarbonate filter (9.2 mm thick). The absorption was measured immediately before the start of UV exposure, and at fixed time intervals (2.5 ml of the solution was withdrawn for the absorption measurements at each time). The absorption measurements were performed using a PerkinElmer Lambda Bio 40 UV/VIS spectrometer.

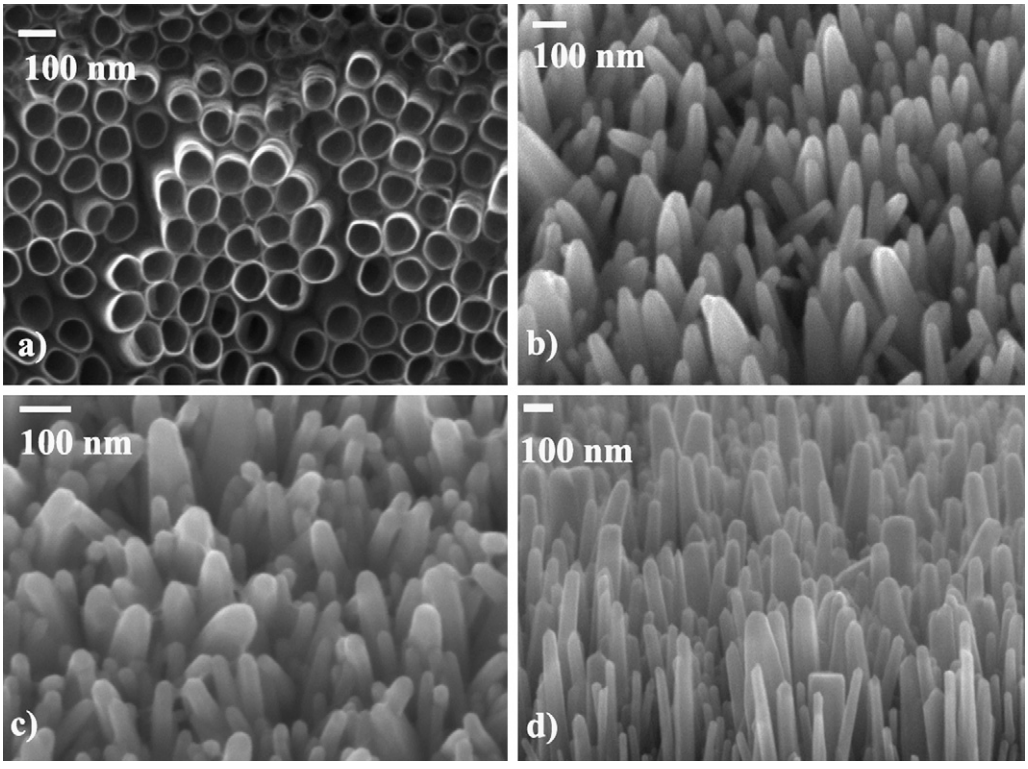

Fig. 2. SEM images of (a) TiO_2 nanotubes; top view, (b) ZnO nanorods, (c) ZnO/TiO_x nanorods and (d) ZnO/Al_xO_y nanorods; tilted view.

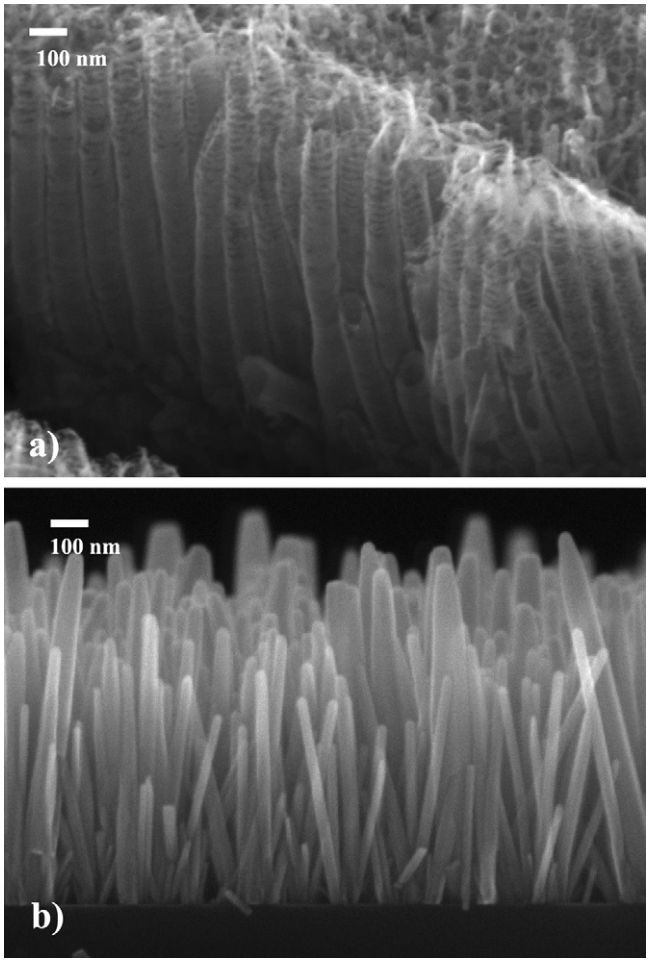

Fig. 3. Cross-section SEM images of (a) TiO_2 nanotubes and (b) ZnO nanorods.

3. Results and discussion

The morphology of the obtained 1D TiO_2 and ZnO nanostructures was examined using SEM, and the results are shown in Fig. 2. The ZnO nanorods exhibited diameters in the range ~30–60 nm. No significant change in morphology was detected after shell deposition, although presence of Al and Ti (at concentrations below 1 at%) was detected by energy dispersive X-ray (EDX) spectroscopy. The inner diameter of titania nanotubes was ~85 nm, and the outer diameter was ~100 nm. The synthesis conditions were chosen to produce a similar length of nanostructures (~900–1200 nm for TiO_2, ~800–900 nm for ZnO), as shown in Fig. 3. The titania nanotubes obtained by anodization are perpendicular to the substrate and closely packed, in agreement with previous work [20,21]. The ZnO nanorods also exhibited mostly perpendicular orientation, but in this case some misaligned rods can also be observed. In general, ZnO samples exhibit larger dispersion of nanorod sizes and alignment compared to the TiO_2 nanotube samples. BET surface area of the samples was 42.4 m^2/g for TiO_2 nanotube samples, and 28.8 m^2/g for ZnO nanorod samples.

TEM images of ZnO nanorods with different shells are shown in Fig. 4. It can be observed that TiO_x forms thicker and more uniform shells, while for Al_xO_y the coverage of the nanorods by alumina shell is incomplete. In both cases the shell thickness is of the order of several nanometer, with some thicker parts of the order of ~10–20 nm. For TiO_x the rods appear to be entirely covered by the shell, while for Al_xO_y there are some bare parts of the rods. The PL spectra of ZnO nanorods with and without shells are shown in Fig. 5. PL emission

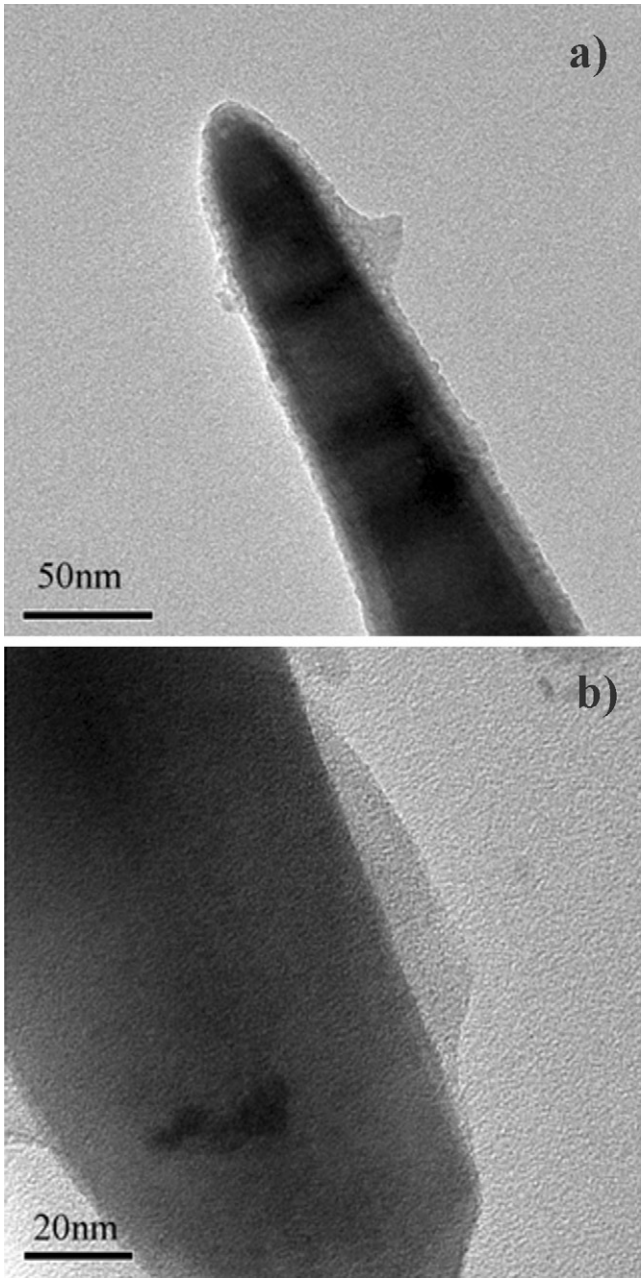

Fig. 4. TEM images of (a) ZnO/TiO_x nanorods and (b) ZnO/Al_xO_y nanorods.

from titania nanotubes prepared by different methods in violet [24], UV–violet [25,26] and blue [24] spectral ranges has been previously reported. However, under experimental conditions in our work, no measurable signal was obtained from TiO_2 nanotubes. The emission from ZnO was affected by the presence of a shell and the type of shell material. All the ZnO nanorods exhibited near-band-edge UV emission and visible emission which is typically attributed to defects [27–29]. The strongest emission intensity can be observed from the bare ZnO nanorods, while nanorods with alumina shell exhibit similar UV-to-visible emission ratio but with lower intensity. This indicates an increase in nonradiative defects with the deposition of a shell. In the case of titania shell, we can observe not only an overall decrease in the emission intensity, but also a decrease in the UV-to-visible emission ratio and the red shift of the defect emission peak. The origin of the defect emission has not been conclusively established [27], but there are indications that in hydrothermally grown samples it is related to the presence of surface adsorbates,

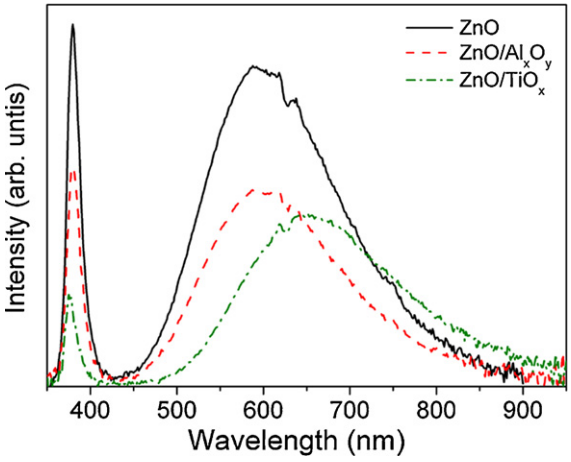

Fig. 5. PL spectra of ZnO, ZnO/TiO_x and ZnO/Al_xO_y nanorods.

such as OH groups [28], and that it possibly originates from defect complexes rather than single point defects [28,29].

Degradation of methyl orange (value of absorption maximum normalized by the absorption maximum at 0 min as a function of time) under UV and simulated solar illumination are shown in Figs. 6 and 7, respectively. It can be observed that ZnO nanorods exhibit comparable (UV) or slightly better (simulated solar illumination) performance than titania nanotubes. This is in agreement with comparisons of ZnO and TiO_2 nanoparticles [8]. For both materials, no activity is observed in any samples when the illumination below 400 nm is blocked by a polycarbonate filter. Since the surface area of TiO_2 nanotubes is somewhat higher compared to ZnO nanorods, while photocatalytic performance is similar or better for ZnO nanorods, it can be concluded that ZnO nanorods represent a promising photocatalytic material. The difference in the performance of ZnO and TiO_2 under UV only and simulated solar illumination likely originates from the differences in the absorption spectra of the two materials. Differences in the native defects could also possibly contribute to different performance under different illumination sources.

For different shell structures, we can observe that titania shell exhibited poorer performance, while alumina shell resulted in comparable performance under UV and somewhat smaller photocatalytic activity under simulated solar illumination. A small difference in performance and photoluminescence with alumina shell could be due to incomplete coverage of the nanorod with the

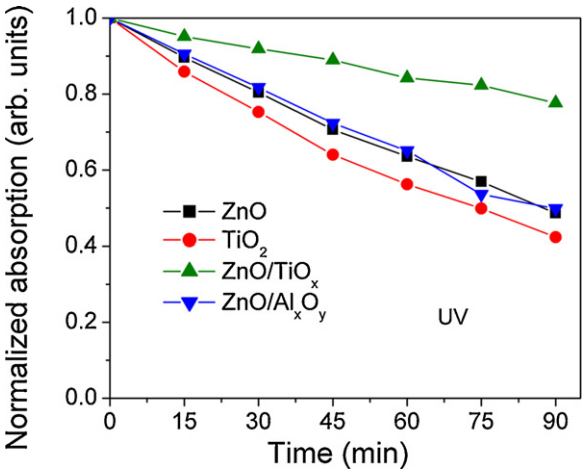

Fig. 6. Degradation of methyl orange under UV illumination.

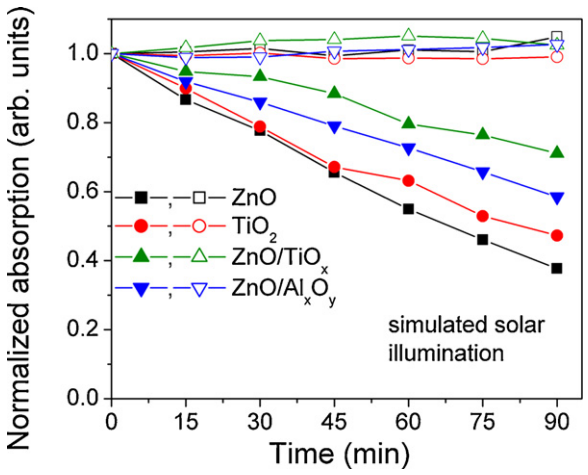

Fig. 7. Degradation of methyl orange under simulated solar illumination. The open symbols indicate measurement with polycarbonate filter, the closed symbols indicate measurements without a filter.

shell. Another possible reason is the difference in native defects in ZnO nanorod due to different annealing temperature for the shell preparation for alumina and titania. This is different from a previous report on the effect of titania and alumina shells on the recombination rates and photovoltaic performance of ZnO-nanorod based solar cells, where improvement was observed for titania but not for alumina shell [18]. This is likely due to the differences in the shell deposition method, atomic layer deposition in previous work [18] and simple solution-based method in this work. It is well-known that native defects affect the trapping and recombination of the photogenerated carriers [30]. Furthermore, the recombination of the photogenerated carriers in ZnO/titania core–shell-based solar cells has been shown to depend on the crystallization, morphology and the continuity of the shell [31]. Since from the PL spectra we can conclude that the titania shell results in significant change in the defect types and densities, decrease in the photocatalytic activity likely originates from the increase in the native defects in ZnO (due to annealing temperature used [28,29]) or at ZnO/titania interface.

4. Conclusions

1D nanostructure arrays of TiO_2 and ZnO exhibited comparable photocatalytic performance. However, coating of titania shell on ZnO resulted in the worsening of photocatalytic performance, which could be attributed to the increased defects. The performance is expected to be dependent on the method of coating the shell and its thickness, which could affect the formation of defects at ZnO/TiO_x interface. On the other hand, only a small decrease in photocatalytic activity under simulated solar illumination and comparable activity under UV illumination is observed for alumina shells.

Acknowledgements

This work is partly supported by the University Development Fund and Strategic Research Theme, the University of Hong Kong and RGC CRF CityU6/CRF/08. The authors would like to thank Prof. Raymond W.Y. Wong from Hong Kong Baptist University for the BET surface area measurements.

References

[1] U.I. Gaya, A.H. Abdullah, J. Photochem. Photobiol. C9 (2008) 1–12.
[2] M.D. Hernández-Alonso, F. Fresno, S. Suárez, J.M. Coronado, Energy Environ. Sci. 2 (2009) 1231–1257.

[3] S. Rehman, R. Ullah, A.M. Butt, N.D. Gohar, J. Hazard. Mater. 170 (2009) 560–569.
[4] Y.J. Zhang, X.F. Li, X.S. Hua, N.H. Ma, D. Chen, H.W. Wang, Scr. Mater. 61 (2009) 296–299.
[5] A.G. Kontos, A. Katsanaki, T. Maggos, V. Likodimos, A. Ghicov, D. Kim, J. Kunze, C. Vasilakos, P. Schmuki, P. Falaras, Chem. Phys. Lett. 490 (2010) 58–62.
[6] C.J. Lin, Y.-T. Lu, C.-H. Hsieh, S.-H. Chien, Appl. Phys. Lett. 94 (2009) 113102.
[7] X.M. Wu, Y.H. Ling, L. Liu, Z.H. Huang, J. Electrochem. Soc. 156 (2009) K65–K71.
[8] C. Hariharan, Appl. Catal. A 304 (2006) 55–61.
[9] X.Y. Li, F.H. Zhao, J.X. Fu, X.F. Yang, J. Wang, C.L. Liang, M.M. Wu, Cryst. Growth Des. 9 (2009) 409–413.
[10] T.J. Kuo, C.N. Lin, C.L. Kuo, M.H. Huang, Chem. Mater. 19 (2007) 5143–5147.
[11] S. Janitabar Darzi, A.R. Mahjoub, J. Alloys Compd. 486 (2009) 805–808.
[12] Q. Xiao, L.L. Ouyang, J. Alloys Compd. 479 (2009) L4–L7.
[13] Y.Z. Li, W. Xie, X.L. Hu, G.F. Shen, X. Zhou, Y. Xiang, X.J. Zhao, P.F. Fang, Langmuir 26 (2010) 591–597.
[14] A. Dodd, A. McKinley, T. Tsuzuki, M. Saunders, J. Alloys Compd. 489 (2010) L17–L21.
[15] C. Xu, L.X. Cao, G. Su, X.F. Qu, Y.Q. Yu, J. Alloys Compd. 497 (2010) 373–376.
[16] N. Kaneva, I. Stambolova, V. Blaskov, Y. Dimitriev, S. Vassilev, C. Dushkin, J. Alloys Compd. 500 (2010) 252–258.
[17] M. Bizarro, Appl. Catal. B 97 (2010) 198–203.
[18] M. Law, L.E. Greene, A. Radenovic, T. Kuykendall, J. Liphardt, P.D. Yang, J. Phys. Chem. B 110 (2006) 22652–22663.
[19] K. Shankar, J.L. Basham, N.K. Allam, O.K. Varghese, G.K. Mor, X.J. Feng, M. Paulose, J.A. Seabold, K.S. Choi, C.A. Grimes, J. Phys. Chem. C 113 (2009) 6327–6359.
[20] K.S. Raja, T. Gandhi, M. Misra, Electrochem. Commun. 9 (2007) 1069–1076.
[21] K. Shankar, G.K. Mor, H.E. Praksam, S. Yoriya, M. Paulose, O.K. Varghese, C.A. Grimes, Nanotechnology 18 (065707) (2007) 1–11.
[22] L.E. Greene, M. Law, D.H. Tan, M. Montano, J. Goldberger, G. Somorjai, P.D. Yang, Nano Lett. 5 (2005) 1231–1236.
[23] M. Law, L.E. Greene, J.C. Johnson, R.J. Saykally, P.D. Yang, Nature Mater. 4 (2005) 455–459.
[24] Y. Yang, X.H. Wang, C.K. Sun, L.T. Li, J. Appl. Phys. 105 (094304) (2009) 1–5.
[25] M.A. Khan, H.T. Jung, O.B. Yang, Chem. Phys. Lett. 458 (2008) 134–137.
[26] M.A. Khan, H.T. Jung, O.B. Yang, J. Phys. Chem. B 110 (2006) 6626–6630.
[27] A.B. Djurišić, Y.H. Leung, Small 2 (2006) 944–961.
[28] A.B. Djurišić, Y.H. Leung, K.H. Tam, Y.F. Hsu, L. Ding, W.K. Ge, Y.C. Zhong, K.S. Wong, W.K. Chan, H.L. Tam, K.W. Cheah, W.M. Kwok, D.L. Phillips, Nanotechnology 18 (095702) (2007) 1–8.
[29] K.H. Tam, C.K. Cheung, A.B. Djurišić, C.C. Ling, C.D. Beling, S. Fung, W.M. Kwok, Y.H. Leung, W.K. Chan, D.L. Phillips, L. Ding, W.K. Ge, J. Phys. Chem. B 110 (2006) 20865–20871.
[30] Y.H. Zheng, C.Q. Chen, Y.Y. Zhan, X.Y. Lin, Q. Zheng, K.M. Wei, J.F. Zhu, Y.J. Zhu, Inorg. Chem. 46 (2007) 6675–6682.
[31] M.L. Wang, C.G. Huang, Q.J. Yu, W. Guo, Q.F. Huang, Y. Liu, Z. Huang, J.Q. Huang, H. Wang, Z.H. Deng, Appl. Phys. Lett. 94 (263506) (2009) 1–3.